UCRL-JC-120508
PREPRINT

# Oxide Vapor Distribution from a High-Frequency Sweep E-Beam System

**Robert Chow**
**Patricial L. Tassano**
**Nick Tsujimoto**

**This paper was prepared for submittal to the**
**38th Annual Technical Conference of the Society of Vacuum Coaters**
**Chicago, Illinois, April 2–7, 1995**

**March 1, 1995**

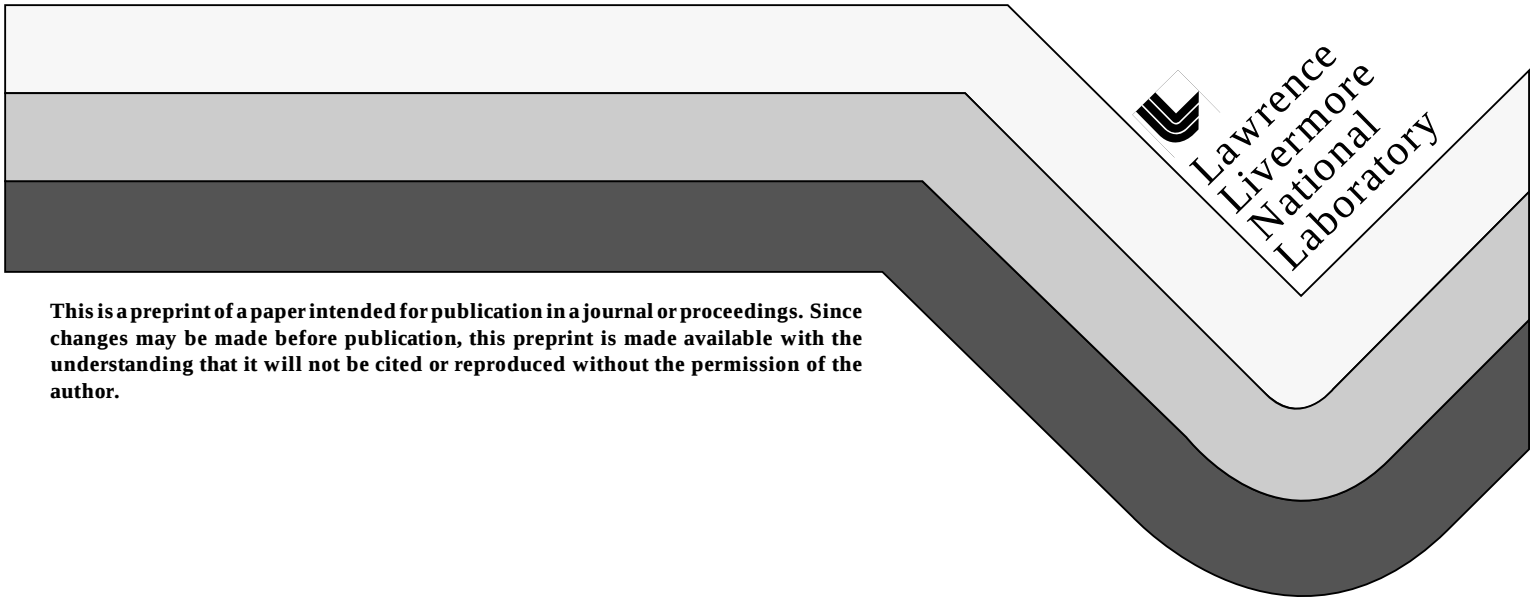

# Oxide vapor distribution from a high-frequency sweep e-beam system

Robert Chow and Patricia L. Tassano
Lawrence Livermore National Laboratory
Livermore, CA USA

Nick Tsujimoto
MDC Vacuum Products Corporation
Hayward, CA USA

Keywords: Electron beam source, Hafnia, Experimental Design, Thickness

## ABSTRACT

Oxide vapor distributions have been determined as a function of operating parameters of a high frequency sweep e-beam source combined with a programmable sweep controller. We will show which parameters are significant, the parameters that yield the broadest oxide deposition distribution, and the procedure used to arrive at these conclusions. A design-of-experimental strategy was used with five operating parameters: evaporation rate, sweep speed, sweep pattern (pre-programmed), phase speed (azimuthal rotation of the pattern), profile (dwell time as a function of radial position). A design was chosen that would show which of the parameters and parameter pairs have a statistically significant effect on the vapor distribution. Witness flats were placed symmetrically across a 25" diameter platen. The stationary platen was centered 24" above the e-gun crucible. An oxide material was evaporated under 27 different conditions. Thickness measurements were made with a stylus profilometer. The information will enable users of the high frequency e-gun systems to optimally locate the source in a vacuum system and understand which parameters have a major effect on the vapor distribution.

## INTRODUCTION

High frequency sweep e-beam sources and programmable beam controllers are commercial introductions. These e-beam systems come with a variety of built-in beam sweep parameters and patterns. We studied how the material hafnia, $HfO_2$, responds within such an evaporation system. Hafnia is an important material for optical thin film multilayers applications requiring high laser damage threshold.

The dependence of the hafnia vapor distribution with these types of the high sweep frequency e-beam system is unknown. The vapor distribution response is important in locating the e-beam source within a coating chamber. This position becomes more critical when coating thickness uniformity is an issue, such as in coating large aperture optics or using these e-beam sources in large evaporation tanks.

Also, multilayered optical coatings with hafnia tend to scatter light more than multilayers using other refractory, high index oxides. The scatter is caused by ejecta from the hafnia melt [1], and the subsequent growth of nodular defects. Hafnia has a temperature-induced solid state phase transition, which increases the propensity of ejecting particles compared with other low absorption oxides. These nodules also couple to the laser light and is the failure site for laser damage [2]. We hypothesize that the high frequency sweeps and the programmable sweep parameters can minimize the temperature excursions in the hafnia source. Stabilizing the temperature profiles would minimize occurrences of the phase transition and hence reduce defect generation from the source.

The purpose of this study is to determine the hafnia vapor flux distribution and defect generation as a function of the following e-gun operating parameters: evaporation rate, sweep speed, sweep pattern (pre-programmed), phase (azimuthal rotation of the pattern), and profile (dwell time as a function of radial position).

## EXPERIMENTAL SET-UP

An MDC 4000 e-beam evaporation system was installed into a stainless steel vacuum chamber. The e-beam had a Cu turret with four pockets of 6 cc volume. The acceleration voltage was 9.2 kV, which centered the e-beam footprint in the hearth during standby conditions. The chamber was 4' x 4'x 5' in dimension, cryopumped with a CTI Cryo-Torr 400 pump and a Sargent Welch 3133-100 turbo-pump. Base pressures of $1.3 \times 10^{-7}$ Torr were routinely obtained overnight without bake-out.

The source material was hafnia (gray) pellets from EM. The hearth was filled with ≈29 gr. of hafnia pellets per run. Single layers of hafnia were deposited to ≈200 nm. Only an additional new pellet was added to the hafnia skull after every evaporation run.

Oxygen was bled in through a micrometer valve and controlled manually at $2 \times 10^{-4}$ Torr during the hafnia evaporation. A GP500 Bayard-Alpert ion gauge was used to monitor the oxygen pressure. The substrates were not intentionally heated.

The thickness distributions were determined from the coating thicknesses measured on glass witness flats. The witness flats (1.0" sq. x 0.125") were placed at 3" intervals along three diagonals on a stationary plate (see Fig. 1). The diagonals were 60° apart from each other. The plate was 12.5" in diameter and centered 24" above the e-gun hearth. The witness flats were shadow-masked with razor blades to create a sharp step in the coating. The thicknesses were measured with a stylus profilometer. Initially, five thickness measurements were taken on each flat. Then it was later found that the differences between the average thickness values taken from five and two measurements were insignificant. The normalized thicknesses, $T_{exp}$, as described by the equation of a circle, were fitted by a least squares error routine to

$$T_{exp} = C_1x^2 + C_2y^2 + C_3\,xy, \qquad \text{eqn. } \{1\}$$

where the $C_i$ are coefficients and the xy term arises because the circle is skewed.
Thickness distributions for e-beam sources are normally described with the cosine power function, $T_{cos}$,

$$T_{cos} = h^2/(h^2 + r^2)\ \cos^{2N}\ \Phi, \qquad \text{eqn. } \{2\}$$

where h = the throw distance of 2 ft., r is the radial position on the platen, and $\Phi$ is the arctan (r/h) [3]. The exponent N is solved numerically by finding the $N_{min}$ which minimizes the sum, S(N), of the differences between equations {1}and{2},

$$S\,(N_{min}) = \Sigma|T_{exp} - T_{cos}|. \qquad \text{eqn. } \{3\}$$

Defect density was measured on three inch diameter Si wafers of prime quality. The wafers were held 7" from the e-beam source, and had ≈700 nm of hafnia deposition. The Si wafers were scanned along two diameters with a 100x microscope. An average defect density was obtained from measuring 25 sites per Si wafer.

An experimental design strategy minimizes the number of runs needed to evaluate the relative importance of a set number of variables to the properties of interest. The properties of interest were the power of the cosine distribution, N, and the defect density, ρ, generation of the hafnia source. Allowing for interaction and quadratic effects of the variables, 26 runs are needed to determine the coefficients for five variables. Four replicate runs were added to compute an average and a confidence limit at the center of the parameter space.

The experimental design had five variables:

(1) The evaporation rates were R = 2, 6 and 10 Å/s. These slow rates were chosen because they fall in the range typically used in making high laser damage threshold coatings;

(2) the sweep speed settings were S = slow, medium and fast. These sweep frequencies are ≈50, 100 and 200 Hz, respectively;

(3) the pre-programmed sweep patterns, P, were the "Line," "Circle" (which was actually more of a spiral), and "FIG8";

(4) the phase settings (angular rotation velocity of the sweep pattern) were A = Slow, Medium and Fast. These phase settings have rotate the pattern by 7°, 17°, and 27°, respectively, per pattern repetition; and

(5) profile settings of D = 1, 1/R, and $1/R^2$, where the beam dwell time is a function of its radial position.

Table I gives the run sequence, and settings in real and normalized space. Columns 2 to 6 give parameter settings as displayed by the beam sweep controller. Columns 7 to 11 have the same parameter settings in normalized space. Columns 12 and 13 are the exponent N and defect densities ρ, respectively, measured from each run. Replicate runs are #1, 10, 20 and 30. Normalization involved quantifying the "slow, medium and fast" controller settings to "-1, 0 and +1" numerical values. The run sequence was randomized to reduce drift errors. A JMP software application by SAS Institute [4] was used to perform the linear regression analysis and statistics on the flux distribution and defect density.

## DISCUSSION and RESULTS

An example of the experimental flux distribution is given in Fig. 2. The thicknesses were interpolated between the measured values and plotted in order to

visualize the thickness variations on the evaporation plane. One observation was that there was no interference of the e-beam on the evaporating flux as reported in earlier references [5,6]. The previous references were evaporating metals at high rates as opposed to a slow reactive evaporation of oxides in this study.

Linear regression of the data to the power exponent N gave the dependence:

$$N = 1.59 + 0.193\ R - 0.012\ P - 0.011\ D + 0.067\ A + 0.017\ S + 0.022\ R^2 + 0.137\ P^2 + 0.072\ D^2 + 0.037\ A^2 - 0.248\ S^2 + 0.033\ P{\bullet}R + 0.051\ D{\bullet}R + 0.016\ D{\bullet}P - 0.011\ A{\bullet}R + 0.054\ A{\bullet}P + 0.009\ A{\bullet}D + 0.008\ S{\bullet}R + 0.02\ S{\bullet}P - 0.055\ S{\bullet}D - 0.115\ S{\bullet}A, \quad \text{eqn } \{4\}$$

where all the parameters, R, P, D, A, and S are in normalized units ranging from -1 to +1. The replicates taken at the center of the parameter space gave an average power exponent of $N_{ave} = 1.71$ with a 95% confidence limit of ± 0.33. Keeping only the coefficients with t-ratios greater than 2.0, eqn. {4} simplifies greatly to

$$N = 1.59 + 0.193\ R - 0.115\ A{\bullet}S. \quad \text{eqn. } \{5\}$$

Values of R and the product A•S are chosen that lower the power exponent N value. Settings of A•S can be either Fast•Fast or Slow•Slow, for the product corresponds to +1 in normalized space; and the rate R = 2 Å/s, corresponds to a -1 value in normalized space. Figure 3 is a surface contour of the power exponent N as a function of rate and speed, keeping phase at a fast setting. As expected, the low values of N are in the upper right quadrant where rate is 2 Å/s and the speed setting is fast.

The defect density data goes through an identical analysis. The defect density ρ depends on the e-beam system parameters as:

$$\rho = 5.5 - 4.07\ R + 2.03\ P - 1.54\ D - 0.13\ A + 2.86\ S + 1.34\ R^2 + 2.88\ P^2 - 1.67\ D^2 - 0.12\ A^2 + 0.75\ S^2 - 0.98\ R{\bullet}P + 0.31\ R{\bullet}D - 0.93\ R{\bullet}A - 1.63\ R{\bullet}S + 0.41\ P{\bullet}D - 2.55\ P{\bullet}A + 5.41\ P{\bullet}S + 0.79\ D{\bullet}S - 2.52\ D{\bullet}A - 1.42\ S{\bullet}A. \quad \text{eqn. } \{6\}$$

The defect density ranges from 0 to 31 #/mm$^2$. The average defect density measured at the center of the parameter space is 3.2 #/mm$^2$ with a 95% confidence limit of ± 2.7. Eqn. {6} simplifies to:

$$\rho = 5.5 - 4.07\ R + 2.03\ P + 2.86\ S - 2.52\ D\ A - 2.55\ P\ A + 5.41\ P\ S, \quad \text{eqn. } \{7\}$$

where coefficients with t-ratios less than 2.0 are removed. The deposition rate must be increased to lower the defect density, in contrast to a decreasing rate to obtain a broad flux distribution. The JMP applications program indicates that an optimal value for ρ can be found at the low rate, and speed and dwell settings at 0, or a medium value. The Phase and Pattern settings were ambiguous because these values were not close to the normalized parameters of -1, 0 or +1. (The reader must note that the programmable sweep controller has no gradations between Slow, Medium and Fast settings of the phase and pattern controls.) The surface contour plot of defect density as a function of Phase and Pattern, and keeping the other parameters at their optimal values, is shown in Fig. 4. The optimal Phase and Pattern settings are +1 and 0, respectively, in normalized space, or Fast and Medium in real space.

The programmable-high frequency sweep e-beam source should provide more stable temperature profiles in the hafnia source and thereby reduced defect densities. Two-dimensional speed-phase slices were taken through the parameter space at constant rate, pattern and dwell settings. The optimal speed and phase setting for low defect densities are located and listed in Table 2. The deposition rate was kept constant at 10 Å/s because lower rates only increase the defect density (see eqn. {7}). The observation is that there are more Slow speed settings than Fast speed settings. On the other hand, there are more Fast phase settings than Slow phase settings. A possible explanation is that Phase, azimuthal rotation of a pattern, significantly impacts the temperature stability in a hafnia melt. An increased temperature uniformity could occur either by a stirring affect of rotating the e-beam pattern of simply increased areal coverage by the e-beam. Adding a fast azimuthal rotation to the pattern appears to reduce the defect density for the sweep settings listed in Table II.

## CONCLUSIONS

In summary, the evaporation characteristics of hafnia was studied using a high frequency sweep e-beam source combined with a programmable sweep controller. The hafnia flux distribution had a cosine power exponent that ranged from 1.13 to 2.0. The flux distribution was affected by the deposition rate and the cross-term Phase•Speed. The hafnia defect density was found to depend on the deposition rate, Pattern, Speed, Phase•Pattern, Phase•Profile, and Speed•Pattern. The optimal low defect density settings was not compatible with the optimal low exponent values for two reasons. First, the Rate coefficients have opposite signs in the models. Second, the rate term did not occur anywhere else in the two models. In the majority of settings, the

Fast Phase (azimuthal rotation of the sweep pattern) setting reduces the defect density for a given sweep settings.

REFERENCES


1. R. Chow, S. Falabella, G. E. Loomis, F. Rainer, C. J. Stolz, and M. R. Kozlowski, "Reactive evaporation of low defect density hafnia," Appl. Optics, 5567-2274, 1993.

2. R. J. Tench, M. R. Kozlowski, and R. Chow, " Defect geometries and laser-induced damage in multilayer coatings," SPIE vol. 2262, 60-66, 1994.

3. H. K. Pulker, *Coatings on Glass*, 3rd ed., Vol. 6, eqn. 59, Elsevier, Amsterdam, 1987.

4. JMP, ver. 2.0.5, SAS Institute Inc., SAS Campus Dr., Cary, NC 27513.

5. R. J. Hill, ed., *Physical Vapor Deposition*, pg. 46, Temescal, Berkeley, CA, 1986.

6. H. R. Smith, "Deposition distribution and rates from electron-beam-heated vapor sources," Proceedings of the 12th Annual Technical Conference, Society of Vacuum Coaters, 50-54, 1969.


ACKNOWLEDGMENT


This work was performed under the auspices of the U. S. Dept. of Energy by Lawrence Livermore National Laboratory under contract No. W-7405-Eng-48. The authors would like to thank Janet Conrad for meticulously proof-reading the manuscript.


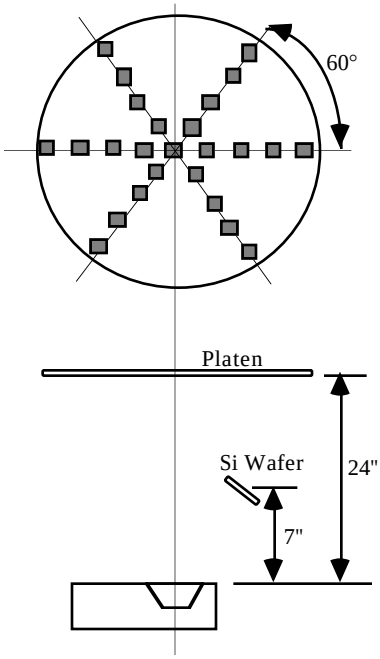


Figure 1: Top and side view of coating fixture. The thicknesses distributions were determined from the hafnia deposited onto the glass substrates.

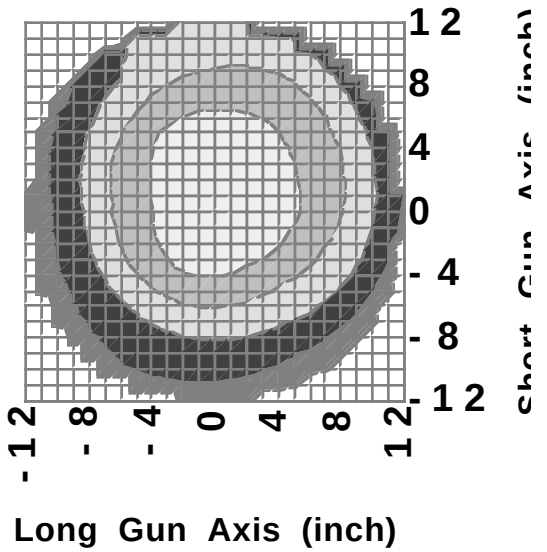


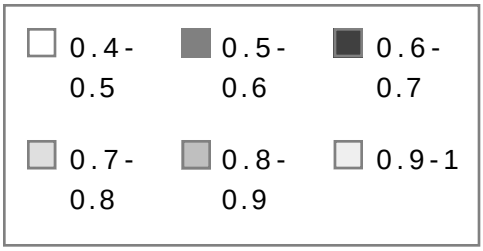


Figure 2: Normalized thickness distribution as measured from the glass witness flats. The electron beam filament is located at (0, 12) on the short and long gun axis, respectively. There is no effect of the e-beam on the flux distribution.

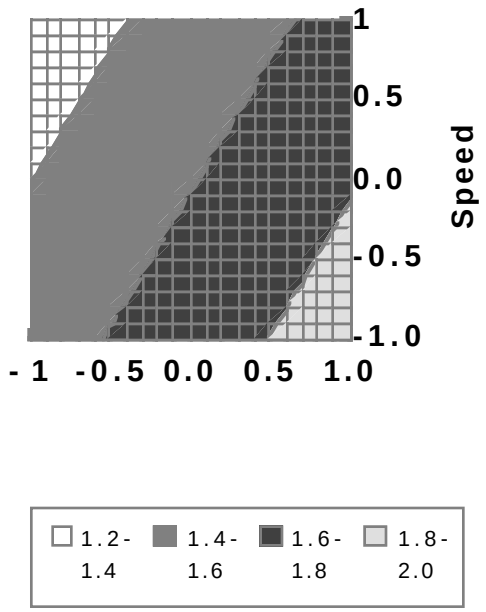


Figure 3: Surface contour plot of the power cosine exponent, N, in terms of normalized rate and speed. The contour plot was generated at a fast phase setting. Low values of N give the broadest vapor distribution. These values occur at low rates and fast speeds.

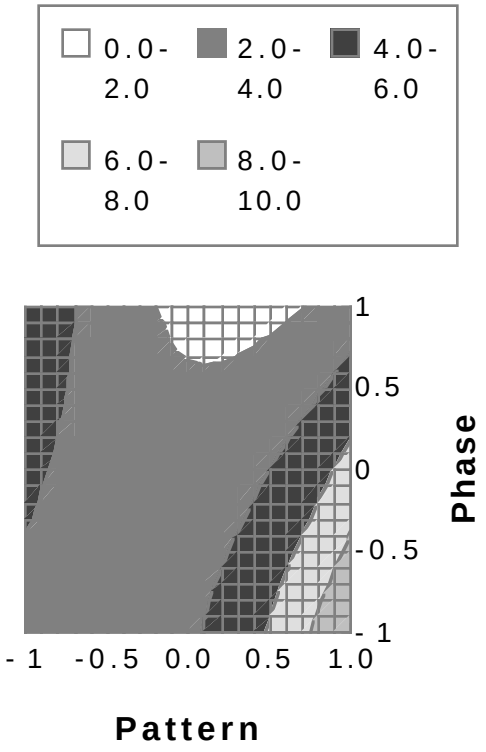


Figure 4: Hafnia defect density surface contour in normalized pattern and phase space. A surface contour was made at optimal settings of Rate, Speed and Dwell. By observation, the optimal settings for the Phase is Fast (+1 in normalized space) and Pattern is Circle (zero in normalized space.

Table I: Design of Experiment Run Parameters

| Run | R | P | D | A | S | R | P | D | A | S | N | ρ |
|---|---|---|---|---|---|---|---|---|---|---|---|---|
| 1 | 6 | Circle | 1/R | Medium | Medium | 0 | 0 | 0 | 0 | 0 | 1.98 | 0.78 |
| 2 | 10 | FIG8 | 1 | Fast | Fast | 1 | -1 | -1 | 1 | 1 | 1.66 | 1.32 |
| 3 | 6 | Circle | $1/R^2$ | Medium | Medium | 0 | 0 | 1 | 0 | 0 | 1.49 | 0.00 |
| 4 | 10 | Line | $1/R^2$ | Fast | Fast | 1 | 1 | 1 | 1 | 1 | 1.85 | 4.66 |
| 5 | 10 | Line | 1 | Fast | Slow | 1 | 1 | -1 | 1 | -1 | 1.86 | 1.00 |
| 6 | 6 | Circle | 1/R | Medium | Fast | 0 | 0 | 0 | 0 | 1 | 1.42 | 10.86 |
| 7 | 2 | Circle | 1/R | Medium | Medium | -1 | 0 | 0 | 0 | 0 | 1.28 | 10.10 |
| 8 | 10 | Circle | 1/R | Medium | Medium | 1 | 0 | 0 | 0 | 0 | 1.84 | 5.83 |
| 9 | 6 | FIG8 | 1/R | Medium | Medium | 0 | -1 | 0 | 0 | 0 | 1.62 | 9.71 |
| 10 | 6 | Circle | 1/R | Medium | Medium | 0 | 0 | 0 | 0 | 0 | 1.76 | 3.30 |
| 11 | 6 | Circle | 1 | Medium | Medium | 0 | 0 | -1 | 0 | 0 | 1.73 | 9.91 |
| 12 | 6 | Circle | 1/R | Slow | Medium | 0 | 0 | 0 | -1 | 0 | 1.35 | 7.38 |
| 13 | 10 | Line | $1/R^2$ | Slow | Slow | 1 | 1 | 1 | -1 | -1 | 1.70 | 2.83 |
| 14 | 2 | Line | $1/R^2$ | Fast | Slow | -1 | 1 | 1 | 1 | -1 | 1.63 | 2.14 |
| 15 | 10 | Line | 1 | Slow | Fast | 1 | 1 | -1 | -1 | 1 | 1.87 | 13.73 |
| 16 | 6 | Circle | 1/R | Fast | Medium | 0 | 0 | 0 | 1 | 0 | 1.80 | 5.63 |
| 17 | 2 | Line | 1 | Slow | Slow | -1 | 1 | -1 | -1 | -1 | 1.13 | 6.22 |
| 18 | 2 | FIG8 | 1 | Slow | Fast | -1 | -1 | -1 | -1 | 1 | 1.71 | 4.66 |
| 19 | 6 | Circle | 1/R | Medium | Slow | 0 | 0 | 0 | 0 | -1 | 1.16 | 0.78 |
| 20 | 6 | Circle | 1/R | Medium | Medium | 0 | 0 | 0 | 0 | 0 | 1.59 | 3.89 |
| 21 | 2 | FIG8 | 1 | Fast | Slow | -1 | -1 | -1 | 1 | -1 | 1.64 | 20.97 |
| 22 | 10 | FIG8 | 1 | Slow | Slow | 1 | -1 | -1 | -1 | -1 | 1.62 | 4.01 |
| 23 | 2 | Line | $1/R^2$ | Slow | Fast | -1 | 1 | 1 | -1 | 1 | 1.31 | 30.96 |
| 24 | 6 | Line | 1/r | Medium | Medium | 0 | 1 | 0 | 0 | 0 | 1.73 | 9.30 |
| 25 | 2 | FIG8 | $1/R^2$ | Slow | Slow | -1 | -1 | 1 | -1 | -1 | 1.38 | 5.98 |
| 26 | 2 | FIG8 | $1/R^2$ | Fast | Fast | -1 | -1 | 1 | 1 | 1 | 1.25 | 6.62 |
| 27 | 10 | FIG8 | $1/R^2$ | Slow | Fast | 1 | -1 | 1 | -1 | 1 | 1.89 | 0.19 |
| 28 | 10 | FIG8 | $1/R^2$ | Fast | Slow | 1 | -1 | 1 | 1 | -1 | 2.00 | 6.02 |
| 29 | 2 | Line | 1 | Fast | Fast | -1 | 1 | -1 | 1 | 1 | 1.48 | 25.26 |
| 30 | 6 | Circle | 1/R | Medium | Medium | 0 | 0 | 0 | 0 | 0 | 1.52 | 5.05 |

Table II: Minimizing defect densities

Optimal Speed and Phase settings for Rate = 10 Å/s and the Pattern and Dwell combinations listed in columns 2 and 3.

| Pattern | Profile | Speed | Phase |
|---|---|---|---|
| Circle | 1 | Medium | Fast |
| Circle | 1/R | All | Fast |
| Circle | $1/R^2$ | Slow | Slow |
| Line | 1 | Slow | Fast |
| Line | 1/R | Slow | Fast |
| Line | $1/R^2$ | Slow | All |
| FIG8 | 1 | Fast | All |
| FIG8 | 1/R | Fast | Fast |
| FIG8 | $1/R^2$ | Fast | Fast |

*Technical Information Department* • **Lawrence Livermore National Laboratory**
**University of California • Livermore, California 94551**